COVID-19: Agent-Based Simulation-Optimization to Vaccine Center Location Vaccine Allocation Problem

Xuecheng Yin [a], Sabah Bushaj [b], Yue Yuan [c] and İ. Esra Büyüktahtakın [d]

[a] Management Science and Information Systems, Oklahoma State University, United States
[b] School of Business and Economics, SUNY Plattsburgh, Plattsburgh, United States
[c] Altfest Personal Wealth Management, New York, United States
[d] Grado Department of Industrial and Systems Engineering, Virginia Tech, Blacksburg, United States

Abstract

This paper presents an agent-based simulation-optimization modeling and algorithmic framework to determine the optimal vaccine center location and vaccine allocation strategies under budget constraints during an epidemic outbreak. Both simulation and optimization models incorporate population health dynamics, such as susceptible (S), vaccinated (V), infected (I) and recovered (R), while their integrated utilization focuses on the COVID-19 vaccine allocation challenges. We first formulate a dynamic location-allocation mixed-integer programming (MIP) model, which determines the optimal vaccination center locations and vaccines allocated to vaccination centers, pharmacies, and health centers in a multi-period setting in each region over a geographical location. We then extend the agent-based epidemiological simulation model of COVID-19 (Covasim) by adding new vaccination compartments representing people who take the first vaccine shot and the first two shots. The Covasim involves complex disease transmission contact networks, including households, schools, and workplaces, and demographics, such as age-based disease transmission parameters. We combine the extended Covasim with the vaccination center location-allocation MIP model into one single simulation-optimization framework, which works iteratively forward and backward in time to determine the optimal vaccine allocation under varying disease dynamics. The agent-based simulation captures the inherent uncertainty in disease progression and forecasts the refined number of susceptible individuals and infections for the current time period to be used as an input into the optimization. We calibrate, validate, and test our simulation-optimization vaccine allocation model using the COVID-19 data and vaccine distribution case study in New Jersey. The resulting insights support ongoing mass vaccination efforts to mitigate the impact of the pandemic on public health, while the simulation-optimization algorithmic framework could be generalized for other epidemics.

Keywords: agent-based simulation; optimization; vaccination center facility location; vaccine allocation; vaccine distribution; mixed-integer programming; COVID-19; SIR model, epidemiological model, supply chain and logistics.

1 Introduction

The Coronavirus Disease 2019 (COVID-19) has caused around 7 million deaths worldwide by May 2023 (JHU, 2021) and 1.2 million only in the United States (US), with the largest death toll in the world (15%). Since December 2020, when people started to get vaccinated, the number of daily deaths (cases) in the US has decreased from about 4,000 (200,000) to 1000 (70,000) by October 21, 2021 (JHU, 2020). The significant drop in both the number of deaths and infections shows that the vaccines are effective in controlling the epidemic. Nevertheless, successful vaccination requires an efficient and timely vaccine distribution process under the limited availability of vaccines, the total budget available, and the uncertain disease growth.

In this paper, we formulate a mixed-integer programming (MIP) model to determine the optimal COVID-19 vaccine allocation strategies under budget and population dynamics constraints. To our best knowledge, our study is the first that consolidates a very detailed agent-based simulation of the disease transmission (Covasim) with a new optimal vaccination center location and vaccine allocation MIP model to address vaccine allocation challenges of an epidemic outbreak. We incorporate service center location and service decision for each center, including the nearby regions served by the center in the optimization model and the number of vaccines allocated to each region. We then extend the ABM presented by Kerr et al. (2021) to incorporate different types of vaccines with one or two shots and forecast disease growth under different vaccination allocation policies. We integrate all those elements into one simulation-optimization framework. The optimization model uses the simulation results as input to generate the optimal vaccine allocation decisions and transfers the optimal decisions into simulation, which populates very detailed health states, such as the number of infections with presymptomatic, mild, severe, and critical conditions, in the following period. We calibrate, validate, and test our simulation-optimization vaccine allocation framework using the COVID-19 data from New Jersey JHU (2020) collected during the middle stages of the pandemic.

Agent-based simulation has been widely used for epidemic control to forecast disease transmission and analyze both pharmaceutical and non-pharmaceutical interventions (see, e.g., Shamil et al. (2021) and Kerr et al. (2021)). The vaccination interventions have also been incorporated into the agent-based simulations (see, e.g., Yin and Büyüktahtakın (2022), Liu et al. (2008), Lee et al. (2010)). Other studies focus on the impact of non-pharmaceutical interventions on controlling the transmission of COVID-19 (Ambikapathy and Krishnamurthy, 2020; Saldaña et al., 2020).

Mathematical optimization approaches have been integrated with epidemiological disease models to optimize resource allocation in the logistics and operation management of controlling infectious diseases (Bertsimas et al., 2021; Büyüktahtakın et al., 2018; Coşgun and Büyüktahtakın, 2018; Kaplan et al., 2003; Kibis et al., 2020; Tanner et al., 2008; Yin et al., 2023b; Zaric and Brandeau, 2001). Dasaklis et al. (2012) and Queiroz et al. (2022) provide detailed reviews of the operations research (OR) models for epidemic resource allocation and supply chain logistics, respectively. The study of Büyüktahtakın et al. (2018) is among the first that integrates operations logistics with epidemiological susceptible- infected-treated-recovered-funeral-buried (SITR-FB) compartment models to optimize resource allocation decisions while projecting potential disease growth scenarios under different treatment logistics decisions. Similar to the study of Büyüktahtakın et al. (2018), Bertsimas et al. (2021) integrate an epidemiological model, the so-called DELPHI, with a facility location optimization model to optimize vaccine site selection and the assignment of the population to different sites with an objective of minimizing deaths with an application to the COVID-19 case in the US. Yin and Büyüktahtakın (2021) develop a multi-stage stochastic programming approach to fair epidemic resource allocation with two new equity metrics. Yin and Büyüktahtakın (2022) present a vaccine allocation and treatment logistics multi-stage stochastic optimization model under risk-averse objectives to analyze the trade-off between the weighted expected loss due to an outbreak and the expected risks associated with experiencing disastrous pandemic scenarios. Coşgun and Büyüktahtakın (2018) present stochastic and approximate dynamic programming algorithms to optimally allocate the limited intervention budget among the HIV disease compartments while minimizing the number of HIV infections and related deaths over a multi-year planning horizon. Yin et al. (2023b) present a new risk-averse stochastic epidemics-ventilator-logistics optimization model to address the resource allocation challenges of mitigating COVID-19, considering the uncertainty in the number of asymptotic cases. They then propose a region-based decomposition to provide bounds on the complex mean-CVaR multi-stage stochastic MIP model and compare those with the scenario dominance bounds of Büyüktahtakın (2022, 2023). In recent years, simulation-optimization has also been used as a powerful tool to optimize simulated and dynamic systems varying from energy to healthcare and agriculture (Bushaj et al., 2022; Nsoesie et al., 2013; Onal et al., 2020).

The majority of existing studies on epidemic control only use agent-based simulations or optimization models separately. In addition, most researches only focus on one side of epidemic control,

either transmission forecasting or optimizing resource allocation strategies. Furthermore, former vaccine center location models ignore vaccination details, such as different types of vaccines, varying number of shots required, and the allocation of the vaccines to pharmacies and small vaccination sites in addition to vaccination centers. Former vaccine center location-allocation models do not consider time-varying demand for vaccines and vaccination willingness rates. We are not aware of any study that considers an agent-based simulation of disease transmission with a supply chain problem, such as the optimal vaccination center location and vaccine allocation, together, as also declared as a research gap in the literature by Queiroz et al. (2022).

There exist location-allocation optimization models that involve a compartmental disease model inside to simulate the disease scenarios, see, e.g., Büyüktahtakın et al. (2018) and Bertsimas et al. (2021). There are also studies that utilize a spatio-temporal disease spread simulation as an input into their location-allocation optimization models, see, e.g., Carr and Roberts (2010) and Ekici et al. (2014). The main differences between our agent-based simulation-optimization approach and the ones in the literature are (i) MIP has a population-level compartmental simulation and disease dynamics equations in the form of a Susceptible-Vaccinated-Infected-Recovered (SVIR) model, while the agent-based model has a very detailed compartmental model and disease contact networks to capture inherent uncertainty in disease progression, (ii) MIP and agent-based simulation models interact iteratively in a loop with forward and backward in the planning horizon, (iii) MIP model is specifically designed for vaccine center location and vaccine allocation and is new because it captures vaccine allocation details that have not been considered in the literature, (iv) the integrated agent-based and MIP model focuses on COVID-19 disease dynamics, and (v) the statistical and visual validation approach jointly validates the results of both optimization and simulation.

Our main methodological contribution is to decompose an extremely challenging problem into two OR methods (optimization and agent-based simulation) involving disease dynamics to take advantage of both approaches. Computational results comparing our simulation-optimization approach with the optimization model without agent-based simulation show that the predictions of simulation-optimization are more robust than the latter, capturing the inherent uncertainty better while tackling with problem complexity. Moreover, both approaches are inspired by epidemiological modeling, innovatively combining traditionally-distinct disciplines of OR and epidemiological modeling to find realistic solutions to the vaccine allocation problem during a pandemic.

2 Simulation-Optimization Modeling Framework

In this section, we discuss the agent-based simulation (Section 2.1), optimization (Section 2.2), and their integration (Section 2.3). The role of the optimization is to determine the optimal vaccine location-allocation decisions, while the goal of the agent-based simulation is to capture the inherent uncertainty in disease dynamics through human contact networks and provide detailed compartmental statistics. Both optimization and agent-based simulation have SIR-type sub-models, but they are not the same. The optimization utilizes a simple, population-level compartmental disease sub-model to project the impacts of various vaccination decisions on the number of infected individuals over a multi-period planning horizon and to optimize its location-allocation decisions accordingly. On the other hand, the simulation utilizes an agent-based individualistic compartmental disease model for COVID-19, which is used to refine and determine the compartmental statistics, such as the numbers of infections and susceptible people, to be used as input into the optimization. The agent-based simulation relies on a very detailed contact network with changing transmission probabilities based on the type of contacts, age, and comorbidity. We then present an algorithm that formally defines the interplay between the optimization and agent-based simulation forward and backward in time over multiple time periods. Utilizing the best features of both optimization and simulation modeling approaches, the vaccine allocation results are obtained from the optimization, while the compartmental disease statistics, e.g., number of cumulative infections, are taken from the agent-based simulation, as presented under Section 3.

2.1 Agent-based Simulation Model

Covasim, is a stochastic agent-based simulator (Covasim (idmod.org)) developed by Kerr et al. (2021) to perform COVID-19 analyses. The ABM involves human behaviors and daily activities to simulate the transmission process of COVID-19 under different intervention strategies, including social distancing, school closures, testing, contact tracing, quarantine, and vaccination. Covasim is shown to provide accurate projections of the number of infections and peak hospital demand under varying intervention measures and has been applied in over a dozen countries, including the US, UK, and Australia, to inform policy decisions. To our knowledge, none of the former works has used Covasim with a mathematical programming approach to inform public policy on COVID-19.

The main purpose of incorporating an ABM, such as Covasim, into our optimization framework is that it can build a realistic model by capturing the stochasticity in the system by expressing the relationship between individual agents in a human population. Individual agents have contact networks (household, school, workplace, and community), as shown in Figure 1, existing conditions, specified viral loads, specified demographics such as age, and different transmission and disease susceptibility rates based on their age. This allows for distinction between agents, implying that two individuals in the same compartment do not have the same characteristics. While some of the special features of different regions, such as social and economic disparities, are not explicitly discussed, their indirect impact on disease transmission has been implicitly captured by the agent-based simulation through various contact networks. The transmission in the simulation is defined based on an agent's interactions with their contacts. Whenever a susceptible individual comes into contact with an infectious individual on a given day, the transmission of the virus occurs with probability β. The more interaction between individuals, the higher the probability of being infected. For instance, a student may go to school and contact their classmates, and adults may go to workplaces and contact their colleagues, bringing the infection from outside to their households. People may also go to public places during daily activities or hang out in the community. We have calibrated the disease transmission parameter (β) for each region and time period to reflect such social and demographic impacts on epidemic growth in New Jersey. A detailed discussion on the calibration of β is given in Appendix Section A1.

Covasim simulates the state of each agent over several discrete time steps using a detailed compartmental model, as shown in Figure 2. At each time step, the simulation calculates the probability that a given agent on a given time step will change from one state to another, such as from susceptible to infected or from critically ill to death, using contact networks, individualistic decisions, and intervention methods. Most disease parameters, such as exposed-to-infectious, infectious-to-symptomatic, and time from infectiousness onset to recovery, are replicated using log-normal distributions. Age-linked susceptibility, progression, mortality, and contact probabilities are defined and used in contact networks. While all parameters and related probability distributions can be found in Kerr et al. (2021), we also present Covasim-related key parameters and their values in Tables A1 and A2 in Appendix Section A1.

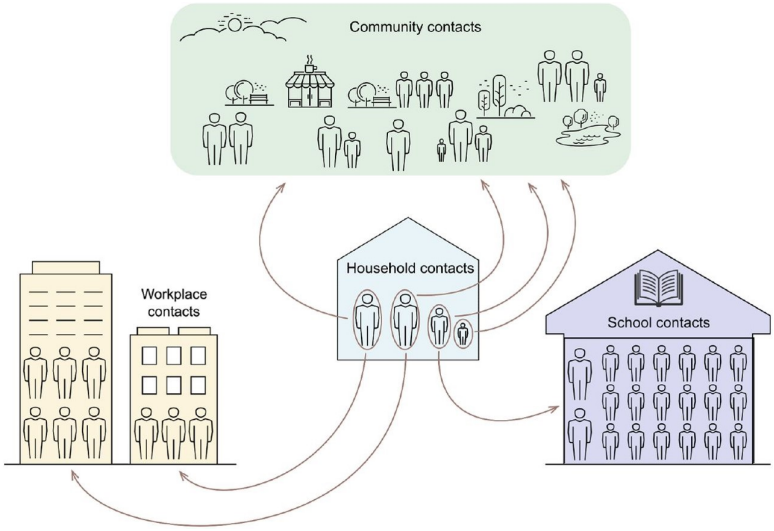

Figure 1: Contact networks for Covasim simulation Kerr et al. (2021).

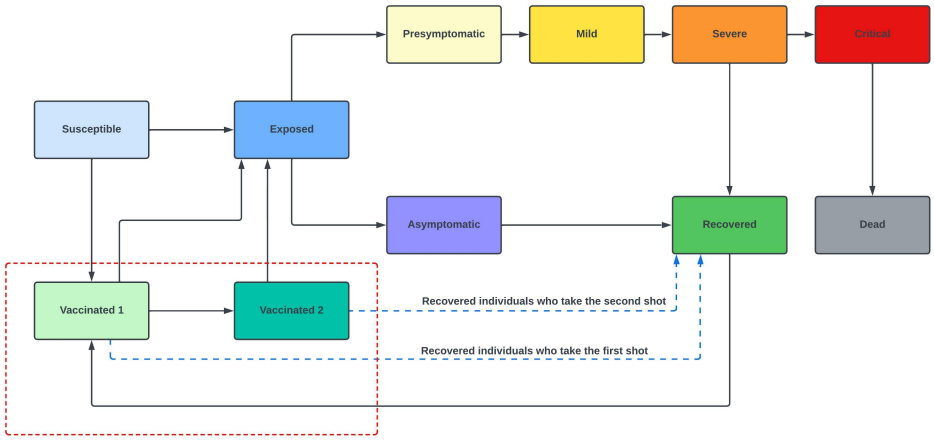

Figure 2: Compartment model that shows the progression of the disease for each agent. The red dashed box and the dashed blue lines show the compartments different than those in Kerr et al. (2021). The details of the compartments are described in Appendix Section A2.

The vaccination compartment is not included in the original Covasim presented in Kerr et al. (2021). Thus, we extend the compartment model presented by Kerr et al. (2021) by adding two vaccination compartments. *Vaccinated 1* represents the individuals that have received the first shot of the vaccine, and *Vaccinated 2* represents the individuals that have received the second shot of the vaccine (2). A proportion of susceptible and recovered individuals receive the first shot of the

vaccine. The individuals who choose the Pfizer and Moderna vaccines receive the second shot after a few weeks of their first shot. The susceptible people who have received the vaccine can still be infected, but their probability of infection is much smaller than the general susceptible population. Given a 90-day planning period, we assume that the recovered individuals do not get infected again. However, we allow recovered people to receive vaccines and move back to the recovered compartment to give flexibility to vaccination policies, as shown in the dashed blue arrows in Figure 2.

2.2 Optimization Model Formulation

This section provides the essential features and assumptions of the optimization model, the associated notations, and the mathematical formulation.

2.2.1 Important Features and Model Assumptions

A few assumptions are made in the formulation of the optimization model. To begin with, the optimization model includes three types of vaccines, which are Pfizer, Moderna, and Janssen, and assumes a vaccine center provides only one vaccine type. The Pfizer and Moderna vaccines include two shots, and the Janssen vaccine only requires one shot. Second, we assume that there are two types of vaccination locations in the model: vaccination centers established only in a few regions and local pharmacies and small vaccination sites, such as healthcare centers and hospitals, that have already been available in each region. The locations of the vaccine centers may vary in size and the number of vaccinations they could administer in a day. We consider the vaccination centers that are set up by the government to provide a quick vaccination to the masses of people, as also declared as type 1 vaccine sites that can vaccinate up to 6,000 people per day (FEMA, 2022). More specifically, we assume that the Pfizer vaccination center has a 6,000 daily vaccine capacity due to the high number of supplies (NJIT, 2021), while the Moderna and Janssen vaccination centers have a 2,000 vaccine capacity each. The local pharmacy and small vaccination sites considered in this study are represented by types 4 and 5 vaccine sites with a limited vaccination capacity of 250 vaccines or less per day, according to FEMA (2022). Based on the data given by Heffernan (2021), the daily vaccine supply capacity upper bound for all local pharmacies and small vaccination sites in a region is set to 10,000. In the implementation, we assume that the total vaccine supply

availability is equal to the total vaccination capacity over established vaccine centers and local pharmacies at each stage. We only consider the total capacity for the local pharmacies and small vaccine sites in each region (county) without specifying their exact locations because we do not model the specific distribution to each small vaccination facility in New Jersey (CDC, 2022). The reason for this is that, first, detailed data on vaccine distribution is currently limited, and second, we are interested in a multi-county-level vaccine allocation in this model. Third, we assume that the people in a region are served by the vaccine centers in the closest nearby region or by the local pharmacies and small vaccination sites in their own region, limited by the number of vaccines distributed to each vaccination unit. The optimization model defines a variable to represent the number and type of each vaccine to be allocated to each vaccine center to serve a region as well as local pharmacies and small vaccine centers in total in each region. Fourth, both vaccine centers and local pharmacies get their vaccines from the vaccine supply warehouse. For a newly-established vaccine center, we calculate the distribution cost from the warehouse to the center by multiplying the unit transportation cost of vaccines by its distance from the vaccine supply warehouse. We add a variable cost of \$1.41 in addition to the unit price of each vaccine allocated to the local pharmacies and small vaccination sites as a unit cost for delivery from the vaccine supply warehouse to them. This unit cost of distributing each vaccine is calculated by dividing the total cold chain cost for the vaccines by the total number of vaccines, according to the information obtained from WHO (2021). The exact location of the supply warehouse for each type of vaccine is unknown. According to Pfizer (2021) and Peter Loftus (2021), the Pfizer and Moderna vaccine manufacturing centers are far from New Jersey. Thus, we assume that the Pfizer and Moderna vaccines are transported from the manufacturing center to the supply warehouse by air. The largest port of New Jersey locates in Essex County (Newark Airport), so, fifth, we assume that the Pfizer and Moderna supply warehouses for New Jersey are in Essex County. The Janssen supply warehouse locates in Somerset County. Sixth, the vaccination willingness rate is defined as the percent population who is willing to accept the COVID-19 vaccination given that the vaccine is provided to them. This rate is estimated as 0.3% per day using the information obtained from NJ.GOV (2021).

SVIR Compartmental sub-model. To incorporate the general disease transmission dynamics and make better vaccine allocation decisions while overseeing their impacts on disease growth, we incorporate disease transmission equations in the optimization model in each region at each stage.

Those equations are formulated based on a simple SVIR compartment flow simulation, as shown in Figure 3. This simplified compartmental disease model is only used in the optimization, where S represents the *Susceptible* compartment in Figure 2. People in S can be infected, moving to the infected compartment I, which includes *Asymptomatic* and *Presymptomatic* people. *V1* and *V2* represent the individuals who received the first dose and second dose of different vaccine types, corresponding to *Vaccinated 1* and *Vaccinated 2* compartments in Figure 2, respectively. The disease transmission rate from $S_{j,r}$ to $I_{j,r}$ at stage j in region r is represented by the parameter $\lambda_{j,r}$, and its value is drawn from a uniform distribution with a range between 0.2 and 0.4. The parameter $\lambda_{j,r}$ does not take into vaccination account, and thus we subtract the number of individuals that are saved by vaccination from the transmission from S to I ($\lambda_{j,r}S_{j,r}$). This approach models the variable impact of the vaccination efforts on disease transmission rather than using a constant transmission between $S_{j,r}$ to $I_{j,r}$. The susceptible individuals can be vaccinated and transferred to *V1* and *V2*. Infected people (I) and people in both *V1* and *V2* can directly transfer to recovered compartment R, depending on the vaccine type. The results for the S, I, *V1*, and *V2* compartments in each region at each stage are only used in the optimization model to generate the vaccine center location and vaccine allocation decisions, while compartmental statistics are refined with fixed vaccine allocation policies in the agent-based simulation. We assume that recovered individuals do not get infected again and are not vaccinated in the optimization model for simplicity.

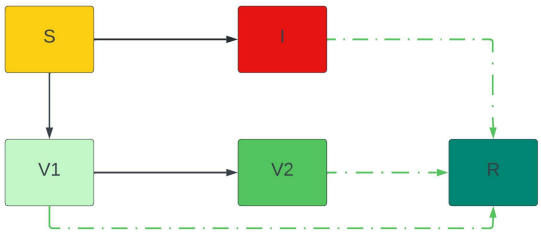

Figure 3: Population compartmental (SVIR) model of optimization.

2.2.2 Notation

In Table 1 below we provide the notations used in the MIP model.

Table 1: Notation.

Sets and Indices:	
J	Set of time periods, $J = \{0, \ldots, \overline{J}\}$.
$\hat{R}$	Set of regions, $\hat{R} = \{0, \ldots, \overline{R}\}$.
ϕ	Set of vaccine type, where $\phi = \{1(\text{Pfizer}), 2(\text{Moderna}), 3(\text{Janssen})\}$.
P	Set of vaccine supply warehouses, $P = \{1, 2, 3\}$.
j	Index for time period, where $j \in J$.
r	Index for region, where $r \in \hat{R}$.
i	Index for vaccine type, where $i \in \phi$.
p	Index for vaccine supply warehouse, where $p \in P$.
State Variables:	
$S_{j,r}$	Susceptible individuals in region r at stage j.
$I_{j,r}$	Infected individuals, including both symptomatic and asymptomatic individuals in region r at stage j.
$V_{j,r}^{i,1}$	Number of people who get the first dose of type $i \in \{1,2\}$ vaccine and a single dose of type $i \in \{3\}$ vaccine in region r at stage j.
$V_{j,r}^{i,2}$	Number of people who get the second dose of type $i \in \{1,2\}$ vaccine in region r at stage j.
Other Parameters:	
b_r^i	Cost of building type i vaccination center in region r.
c^i	Unit cost for each type i vaccine, including the purchase cost.
τ^i	Unit purchase and transporting cost for each type i vaccine from warehouse to local pharmacies and small vaccination centers (LPSVC).
$d_{r,l}$	The distance from the highest populated city in region r to the highest populated city in region l.
$d_{p,r}$	The distance from vaccine supply warehouse p to the highest populated city in region r.
t	Unit transportation cost of vaccines with a truck from the vaccine supply warehouse to a region.
κ_i	number of days between the first and second shot of type $i \in \{1,2\}$ vaccine, where $\kappa_1 = 21$ and $\kappa_2 = 28$.
$G_{j,r}^i$	Vaccination capacity for type i vaccination center at stage j in region r.
H_j^i	Vaccine supply upper bound for type i vaccine at stage j.
$C_{j,r}^i$	Total existing capacity of the local pharmacies and small vaccination sites for type i vaccine at stage j in region r.
$\lambda_{j,r}$	Disease transmission rate from $S_{j,r}$ to $I_{j,r}$ in region r at stage j.
β_r^1	The first shot vaccine acceptance rate, i.e., willingness to get vaccinated, for a two-dose vaccine in region r.
β_r^2	The lower bound of the second shot vaccine acceptance rate for a two-dose vaccine in region r.
β_r^3	The vaccine acceptance rate for the single-dose vaccine in region r.
$\alpha_r^{i,1}$	Daily proportion of individuals who get immunization by the first shot of type i vaccine.
$\alpha_r^{i,2}$	Daily proportion of individuals who get immunization by the second shot of type i two-dose vaccine.
χ	Proportion of infected individuals recovered.
ψ_1	Proportion of individuals who get the first vaccine moving to the recovered compartment.
ψ_2	Proportion of individuals who get the second vaccine moving to the recovered compartment.
n_r	The total number of vaccine centers allocated in region r.
e	Euler's number.
m, k	Parameters that are used to change the value of the logistics function in (1s) and (1t).
π_r	The initial number of susceptible individuals in region r, inputted from the agent-based simulation model.
ϖ_r	The initial number of infections in region r, inputted from the agent-based simulation model.
θ_r^i	The initial number of individuals who have received the first-dose type $i \in \{1,2\}$ vaccine shot in region r.
ϑ_r^i	The initial number of individuals who have received the second-dose type $i \in \{1,2\}$ vaccine shot in region r.
σ_r^i	The initial number of individuals who have received the first and single-dose type $i \in \{3\}$ vaccine shot in region r.
Decision variables:	
x_r^i	Whether to build type i vaccination center in region r ($x_r^i \in \{0,1\}$).
$y_{r,l}$	Whether vaccination center in region r serves people in region l ($y_{r,l} \in \{0,1\}$).
$o_{j,r}^{i,1}$	Number of type $i \in \{1,2\}$ first-dose or number of type $i \in \{3\}$ single-dose vaccines allocated for a newly established center.
$o_{j,r}^{i,2}$	Number of type $i \in \{1,2\}$ second-dose vaccines allocated for a newly established center.
$z_{j,r}^{i,1}$	Number of type $i \in \{1,2\}$ first-dose or number of type $i \in \{3\}$ single-dose vaccines allocated for LPSVC.
$z_{j,r}^{i,2}$	Number of type $i \in \{1,2\}$ second-dose vaccines allocated for LPSVC.

2.2.3 Mathematical Formulation

The mathematical formulation for the optimization model is given below.

$$\min \quad \sum_{j\in J}\sum_{r\in\hat{R}} I_{j,r} \tag{1a}$$

$$\text{s.t.} \quad y_{r,l} \le x_r^i \qquad r,l \in \hat{R}, i \in \{1,2,3\}, \tag{1b}$$

$$\sum_{r\in\hat{R}} y_{r,l} = 1 \qquad \forall l \in \hat{R}, \tag{1c}$$

$$x_k^i + y_{r,l} \le 1 \qquad \forall k,r,l \in \hat{R}, i \in \{1,2,3\}$$

$$(\text{s.t.} \quad d_{k,l} \le d_{r,l}), \tag{1d}$$

$$\sum_{i=1}^{3} x_r^i \le n_r \qquad \forall r \in \hat{R}, \tag{1e}$$

$$S_{0,r} = \pi_r, \quad I_{0,r} = \varpi_r, \quad V_{0,r}^{i,1} = \theta_r^i, \quad V_{0,r}^{i,2} = \vartheta_r^i \quad r \in \hat{R}, i \in \{1,2\},$$

$$V_{0,r}^{i,1} = \sigma_r^i \quad r \in \hat{R}, i \in \{3\}, \tag{1f}$$

$$S_{j+1,r} = S_{j,r} - \lambda_{j,r}S_{j,r} - \sum_{i\in\{1,2\}} (o_{j,l}^{i,1} + z_{j,l}^{i,1}) - (o_{j,l}^{3,1} + z_{j,l}^{3,1})$$

$$j \in J \setminus \{\overline{J}\}, r \in \hat{R}, \tag{1g}$$

$$I_{j+1,r} = I_{j,r} + (\lambda_{j,r}S_{j,r} - \sum_{i\in\{1,2\}} (o_{j,l}^{i,1} + z_{j,l}^{i,1})\alpha_r^{i,1} - \sum_{i\in\{1,2\}} (o_{j,l}^{i,2} + z_{j,l}^{i,2})\alpha_r^{i,2}$$

$$-(o_{j,l}^{3,1} + z_{j,l}^{3,1})\alpha_r^{3,1}) - \chi I_{j,r} \qquad j \in J \setminus \{\overline{J}\},\ r \in \hat{R}, \tag{1h}$$

$$V_{j+1,r}^{i,1} = V_{j,r}^{i,1} + o_{j,r}^{i,1} + z_{j,r}^{i,1} - o_{j,r}^{i,2} - z_{j,r}^{i,2}, j \in J \setminus \{\overline{J}\}, r \in \hat{R}, i \in \{1,2\}, \tag{1i}$$

$$V_{j+1,r}^{i,1} = V_{j,r}^{i,1} + o_{j,r}^{i,1} + z_{j,r}^{i,1} - \psi V_{j,r}^{i,1}, j \in J \setminus \{\overline{J}\}, r \in \hat{R}, i \in \{3\}, \tag{1j}$$

$$V_{j+1,r}^{i,2} = V_{j,r}^{i,2} + o_{j,r}^{i,2} + z_{j,r}^{i,2} - \psi V_{j,r}^{i,2}, \qquad j \in J \setminus \{\overline{J}\}, r \in \hat{R}, i \in \{1,2\}, \tag{1k}$$

$$R_{j+1,r} = R_{j,r} + \chi I_{j,r} + \psi_1 V_{j,r}^{i,1} + \psi_2 V_{j,r}^{i,2}, \qquad j \in J \setminus \{\overline{J}\}, r \in \hat{R}, \tag{1l}$$

$$\sum_{l\in\hat{R}} (o_{j,l}^{i,1} + o_{j,l}^{i,2}) y_{r,l} \le G_{j,r}^i \qquad j \in J, r \in \hat{R}, i \in \{1,2\}, \tag{1m}$$

$$\sum_{l\in\hat{R}} o_{j,l}^{i,1} y_{r,l} \le G_{j,r}^i \qquad j \in J, r \in \hat{R}, i \in \{3\}, \tag{1n}$$

$$\sum_{l\in\hat{R}} (z_{j,l}^{i,1} + z_{j,l}^{i,2}) \le C_{j,r}^i \qquad j \in J, r \in \hat{R}, i \in \{1,2\}, \tag{1o}$$

$$\sum_{l\in\hat{R}} z_{j,l}^{i,1} \le C_{j,r}^i \qquad j \in J, r \in \hat{R}, i \in \{3\}, \tag{1p}$$

$$\sum_{l\in\hat{R}}(o_{j,l}^{i,1}+o_{j,l}^{i,2}+z_{j,l}^{i,1}+z_{j,l}^{i,2})\le H_j^i \qquad \forall j\in J, i\in\{1,2\}, \tag{1q}$$

$$\sum_{l\in\hat{R}}(o_{j,l}^{i,1}+z_{j,l}^{i,1})\le H_j^i \qquad \forall j\in J, i\in\{3\}, \tag{1r}$$

$$\sum_{l\in\hat{R}}(o_{j,l}^{i,1}+o_{j,l}^{i,2}+z_{j,l}^{i,1}+z_{j,l}^{i,2})\ge \frac{m}{1+e^{kj}} \qquad \forall j\in J, i\in\{1,2\}, \tag{1s}$$

$$\sum_{l\in\hat{R}}(o_{j,l}^{i,1}+z_{j,l}^{i,1})\ge \frac{m}{1+e^{kj}} \qquad \forall j\in J, i\in\{3\}, \tag{1t}$$

$$o_{j,l}^{i,1}+z_{j,l}^{i,1}\le S_{j,r}\beta_r^1 \qquad j\in J, \quad r,l\in\hat{R}, i\in\{1,2\}, \tag{1u}$$

$$\beta_r^2 o_{j-\kappa_i,l}^{i,1}\le o_{j,l}^{i,2}\le o_{j-\kappa_i,l}^{i,1} \qquad j\in J, \quad r,l\in\hat{R}, i\in\{1,2\}, \tag{1v}$$

$$o_{j,l}^{i}+z_{j,l}^{i,1}\le S_{j,r}\beta_r^3 \qquad j\in J, \quad r,l\in\hat{R}, i\in\{3\}, \tag{1w}$$

$$\sum_{r\in\hat{R}} b_r^i x_r^i + + \sum_{i\in\{1,2,3\}}\sum_{p\in P}\sum_{r\in\hat{R}} td_{p,r}x_r^i + \sum_{j\in J}\sum_{l\in\hat{R}}\sum_{i\in\{1,2\}} c^i(o_{j,l}^{i,1}+o_{j,l}^{i,2}) + \sum_{j\in J}\sum_{l\in\hat{R}}\sum_{i\in\{3\}} c^i o_{j,r}^i$$
$$+\sum_{j\in J}\sum_{l\in\hat{R}}\sum_{i\in\{1,2\}}\tau^i(z_{j,l}^{i,1}+z_{j,l}^{i,2})+\sum_{j\in J}\sum_{l\in\hat{R}}\sum_{i\in\{3\}}\tau^i z_{j,r}^{i,1}\le\Delta \tag{1x}$$

$$x_r^i, y_{r,l}\in\{0,1\} \qquad i\in I, j\in J, r\in\hat{R}, \tag{1y}$$

$$S_{j,r}, \quad I_{j,r}, \quad o_{j,r}^{i,1}, \quad z_{j,r}^{i,1}\ge 0, \quad j\in J, \quad r\in\hat{R}, \quad i\in\{1,2,3\},$$
$$o_{j,r}^{i,2}, \quad z_{j,r}^{i,2}\ge 0, \quad j\in J, \quad r\in\hat{R}, \quad i\in\{1,2\}. \tag{1z}$$

Objective Function (1a)**.** The objective function (1a) minimizes the total number of infections over all the regions throughout the planning horizon.

Vaccination Center Location and Service Constraints (1b) **-** (1e)**.** Constraint (1b) ensures that region r cannot serve region l if there is no vaccination center that is built in region r. Constraint (1c) represents that only one region with a vaccination center can serve region l. Constraint (1d) ensures that the nearest region with a vaccination center serves region l. Constraint (1e) limits the total number of different types of vaccine centers allocated to region r.

Population Infection Dynamics and Vaccinated Population Constraints (1f) **-** (1l)**.** Constraint (1f) gives the initial number of susceptible and infected individuals generated from the agent-based simulation model presented in Section 2.1 and the initial number of individuals who have received the first-dose of type i ($i\in\{1,2,3\}$) vaccine, as well as the initial number of individuals who have received the second-dose of type i ($i\in\{1,2\}$) vaccine. Constraint (1g) shows that the number of susceptible individuals in region r at stage $j+1$ equals the number of susceptible individuals from the previous stage minus the number of infected individuals in region r at stage j and

minus the number of susceptible individuals who have received the first-dose of type i ($i \in \{1,2\}$) vaccine in region r at stage j, and minus the number of susceptible individuals who have received a single dose of type i ($i \in \{3\}$) vaccine in region r at stage j.

Constraint (1h) implies that the number of infected individuals in region r at stage $j+1$ equals the number of infected individuals from the previous stage plus newly infected individuals from the susceptible compartment minus the number of individuals saved by vaccines, minus infected individuals moving to the recovered compartment. Here, the disease transmission rate from $S_{j,r}$ to $I_{j,r}$, $\lambda_{j,r}$, does not count on vaccinations. To incorporate the variable transmission from S to I, depending on vaccination efforts, we subtract the individuals who are protected by vaccines from susceptible individuals who are newly infected. Constraint (1i) indicates that the number of people who have received the first-dose of type i ($i \in \{1,2,\}$) vaccine in region r at stage $j+1$ equals the number of people who have received the first-dose of type i ($i \in \{1,2\}$) vaccine from the previous stage plus the newly vaccinated people (first dose) minus the number people who have taken the second dose of type i ($i \in \{1,2\}$) vaccine. Constraint (1j) indicates that the number of people who have received the single dose of type i ($i \in \{3\}$) vaccine in region r at stage $j+1$ equals the number of people who have received the single dose of type i ($i \in \{3\}$) vaccine from the previous stage plus the newly vaccinated people (single dose). Constraint (1k) indicates that the number of people who have received the second-dose of type i ($i \in \{1,2\}$) vaccine in region r at stage $j+1$ equals the number of people who have received the second-dose of type i ($i \in \{1,2\}$) vaccine from previous stage plus the newly vaccinated people with the second dose. Constraint (1l) indicates that the number of recovered people in region r at stage $j+1$ equals the number of recovered people from the previous stage plus the number of newly recovered people from the infected compartment and those who transfer from vaccinated compartments.

Vaccine Logistics, Capacity and Budget Constraints (1m) **-** (1x)**.** Constraints (1m) and (1n) ensure that the total number of each type of vaccine allocated to the new vaccine centers in region r at stage j should be smaller than or equal to the vaccine capacity upper bound of the vaccination center in region r. Constraints (1o) and (1p) ensure that the total number of each type of vaccine allocated to local pharmacies and small vaccine sites in region r at stage j should be smaller than or equal to the vaccine capacity upper bound for the two- and single-dose vaccine types, respectively. Constraints (1q) and (1r) ensure that the total number of each type of vaccine supplied to the

new vaccine centers and local pharmacies (and small vaccination sites) over all regions at each stage j should be smaller than or equal to the vaccine supply upper bound at stage j, respectively. Constraints (1s) and (1t) indicate that the total number of each type of vaccine supplied to the new vaccine centers and the existing vaccine locations over all regions at each stage j should be greater than or equal to the vaccination lower bound at stage j. The vaccination lower bound (total demand in all regions) at each stage j is represented by an exponential function reaching an asymptote over time. This function represents a high demand in the initial stages of vaccination which reduces and reaches a constant state as time progresses. Constraint (1u) indicates that the total number of people who have received the first shot of type i ($i \in \{1, 2\}$) vaccine should be smaller than or equal to the people who are willing to be vaccinated, i.e., it is bounded above by the susceptible population times the vaccine willingness rate. Constraint (1v) implies that the total number of people vaccinated by the second shot of type i ($i \in \{1, 2\}$) vaccine should be greater than or equal to the lower bound of the people who are willing to be vaccinated but smaller than or equal to the people who have received the first shot κ_i days before the second shot. Constraint (1w) represents that the total number of people vaccinated by type i ($i \in \{3\}$) vaccine should be smaller than or equal to the people who are willing to be vaccinated by the single-dose vaccine.

Constraint (1x) represents budget limitations. Constraint (1x) ensures that the total fixed and variable costs associated with vaccine centers as well as local pharmacies and small vaccination sites over all regions throughout the whole planning horizon should be smaller than or equal to a certain budget level. The first four terms correspond to the cost of establishing vaccination centers, the logistics distribution cost from the vaccine supply warehouses to vaccine centers, and the purchase cost of vaccines that are distributed to the newly established vaccine centers for both double and single-shot types, respectively. The fifth and sixth terms correspond to the purchase and distribution cost of vaccines that are allocated from warehouses to local pharmacies and small vaccination sites.

Integrality and Non-Negativity Constraints (1y) - (1z). Constraints (1y) and (1z) are variable restrictions. Specifically, constraint (1y) indicates that x_r^i and $y_{r,l}$ are binary variables. Constraint (1z) implies that the number of susceptible individuals, the number of infected individuals, and the number of each vaccine type allocated to centers and local pharmacies should be greater than or equal to 0. We perform linearization, as described in Appendix Section A3 to convert the full non-linear optimization model (1a)–(1z) into an MIP and use this MIP for the rest of the paper.

2.3 Simulation-Optimization Methodology

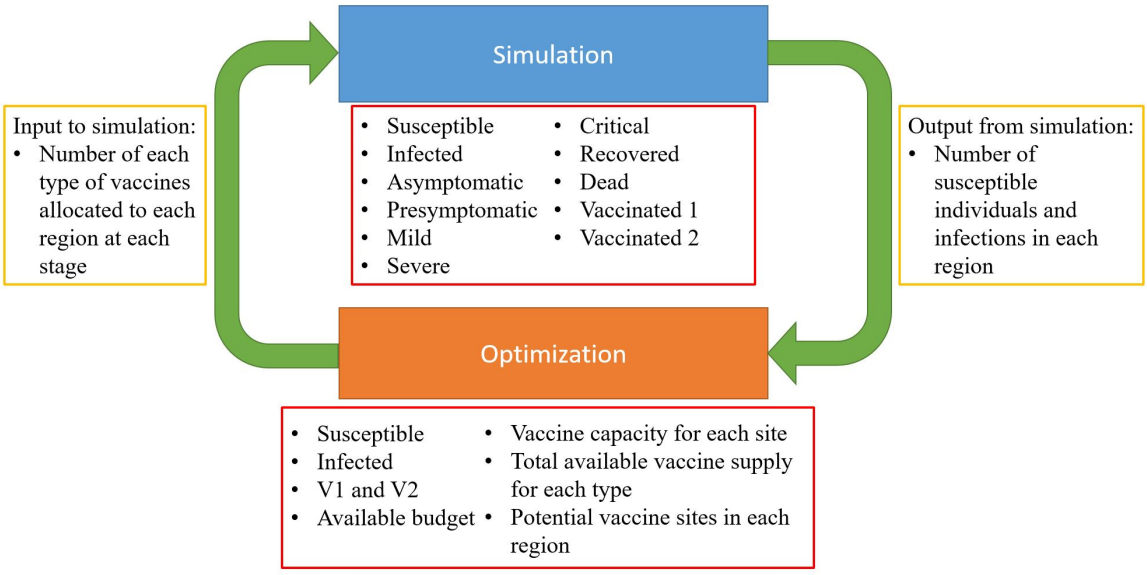

Figure 4: The loop of the simulation-optimization model.

In this paper, we introduce a simulation-optimization approach to address the vaccination facility location and vaccine allocation challenges of COVID-19. We extend the Covasim agent-based model of COVID-19 and combine it with a new vaccination center and vaccine-allocation optimization model. As shown in Figure 4, the integrated model runs in a loop, where the simulation model forecasts the disease transmission and imports the results into the optimization model presented in Section 2.2. The optimization model also includes a simple SVIR model to project the potential disease-growth scenarios in its multi-period planning horizon while optimizing the optimal vaccination center locations and vaccine allocation among each region. The optimization sends the vaccine allocation results back to the simulation model to estimate the number of infections in the future. Specifically, the simulation model uses the number of initial susceptible and infected individuals to forecast the number of susceptible and infected individuals, presymptomatic and asymptomatic individuals, as well as the mild, severe, critical, recovered, and dead individuals for each stage in the current planning horizon. The forecast numbers of susceptible and infected individuals are imported into the optimization model. The optimization model incorporates the available budget, potential vaccine sites in each region, vaccine capacity for each site, and total available vaccine supply for each vaccine type to generate the optimal vaccination center location and vaccine allo-

cation while minimizing the total number of infections in the considered regions. The optimization results include the number of people that are supposed to be vaccinated in vaccination centers, local pharmacies, and small vaccination sites at each future stage in each region. Then these parameters are fed into the simulation model to simulate the number of susceptible and infected individuals for the next periods. We present the step-by-step implementation of the optimization and simulation loops interactively in Algorithm 1 in Appendix Section A4.

In addition, a simulation replication experiment is performed to study the influence of randomness on the agent-based simulation in Appendix Section A5. We run 10 replications for the simulations and use the mean value as the input in the optimization model. We compare the results of replications with our previous results in Figures A3-A5, and the trajectories are found visually close to each other. Since replications require extensive computational effort without much benefit in the output, we use a single simulation for all the results in the main manuscript.

We compare the results of simulation-optimization with the optimization model without simulation in Appendix Section A6. In this section, Figures A6-A8 show that the optimization model projects a similar prediction with simulation-optimization at the beginning, but the number of infections significantly increases later in the time horizon. Therefore, the prediction of simulation-optimization is robust compared to the optimization model without the agent-based simulation.

3 Case Study Results

We apply our simulation-optimization framework described in Section 2.3 to all the counties in New Jersey. The case study data used to formulate and test the model is presented in Appendix Section A7. The data includes the population for each county in New Jersey State, the number of infections over time for each county in New Jersey State, the logistics cost, and the cost of vaccines. The agent-based simulation presented in Section 2.1 is applied to each county separately to fine-tune disease dynamics, while the optimization model in Section 2.2 is applied to all counties at the same time to optimize resource allocation. We solve the optimization model to generate the results of the optimal vaccination center locations and the allocation of vaccines, including Pfizer, Moderna, and Janssen. Then we use the results generated by the optimization model as the inputs of the simulation model. We incorporate vaccination in the Covasim model, as shown in Figure 4. The vaccination includes the first and second shots for Pfizer and Moderna vaccines and a single shot

for the Janssen vaccine. We solve the model for a 90-day period, a planning horizon from March 1, 2021, to May 30, 2021. The optimization model is solved using CPLEX 20.1 on a desktop computer running with an Intel i7 CPU and 64.0 GB of memory. The simulation model is run on the same desktop computer in PyCharm Edu (using python language).

We first present the validation results of the simulation-optimization model in Appendix Section A8. Under Sections A9 and 3.1, we fix only one Pfizer vaccination center in Essex county, similar to the validation experiments, and test our model under different budget levels varying from limited to ample. In those sections, we analyze the distribution of different types of vaccines to the vaccination center as well as local pharmacies and small vaccine centers. We use $\$5M$ as a limited budget level, $\$10M$ as a medium budget level, and we do not put a budget restriction under the ample budget. However, under the ample budget scenario, the number of people being vaccinated is bounded by the number of people willing to be vaccinated in each region and the total vaccination capacity.

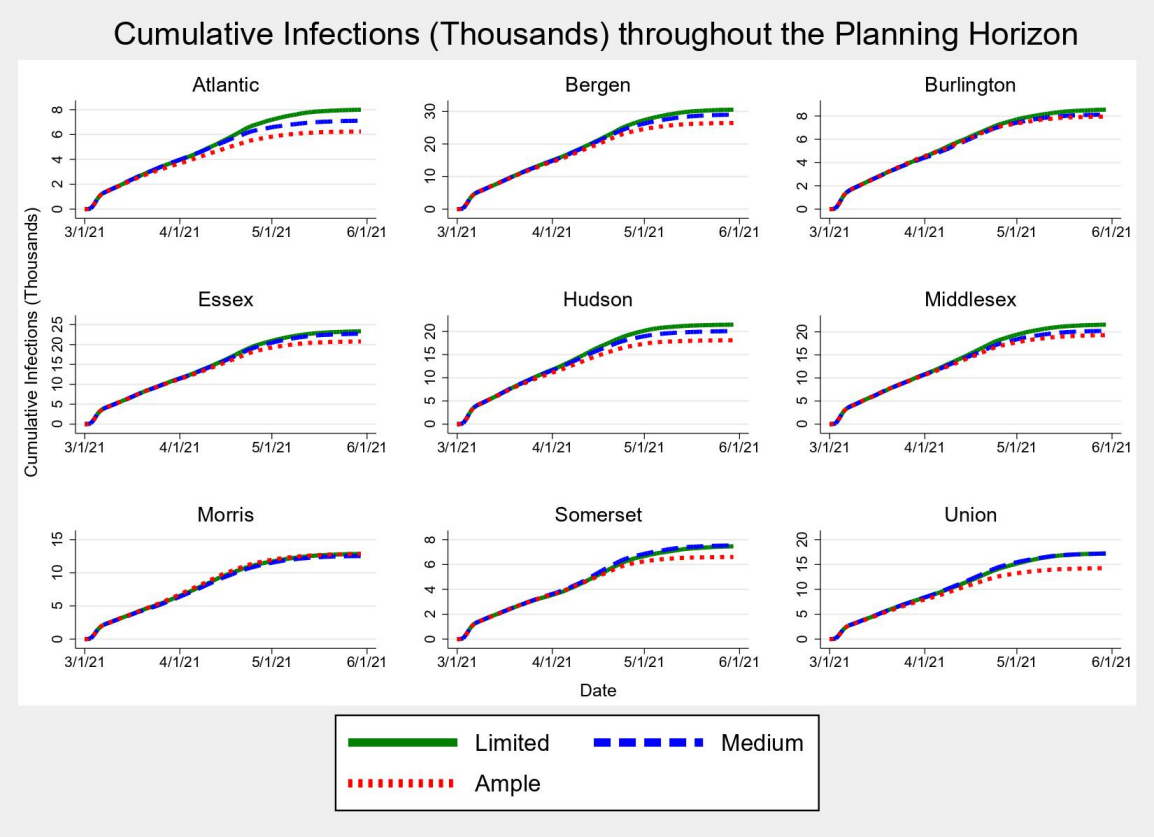

Figure 5: New Jersey cumulative infections under different budget levels. The total cumulative infections are given only from March 1, 2021, to May 30, 2021.

Figure 5 shows the number of cumulative infections under different budget levels for the nine most populated counties in New Jersey. The number of cumulative infections under all three different budget levels for all the counties in New Jersey are shown in Figures A15, A16, and A17 in Appendix Section A9. All the results regarding the number of infections are taken from the simulation results, while all results regarding the number of vaccines allocated refer to the optimization model's results.

3.1 Number of Vaccines Allocated to Each County

The number of vaccines allocated to each county under a limited, medium, and ample budget level is presented in Tables 2, A9, and A10, respectively. Based on the results in those three tables, the cumulative proportion of people vaccinated at the end of the time period is 12.4%, 21.7%, and 32.5% for the limited, medium, and ample budgets, respectively. The columns of each table present the county, the population and vaccination proportions of each county with respect to all counties, the percent difference between the population and vaccination proportions, the total vaccines allocated to each county, the proportion of the vaccines allocated to each county, and the number of first and second doses of each type of vaccines allocated to each county, respectively. Figure 6 shows the proportion of each type of vaccine allocated under different budget levels. In this section, while the model fixes one Pfizer vaccine, we present all types of vaccines allocated to not only the vaccine center but also local pharmacies and small vaccination sites.

Table 2: Vaccine Allocation under Limited Budget Level

County	Population Proportion (%)	Vaccine	Difference	Total Vaccine Dose	Pfizer First Dose	Pfizer Second Dose	Moderna First Dose	Moderna Second	Janssen
Atlantic	3.1%	3.6%	-0.5%	38,789	4,500	1,083	6,493	2,676	24,037
Bergen	10.3%	9.5%	0.8%	103,971	4,500	1,082	12,072	7,138	79,179
Burlington	5.1%	5.1%	0.0%	56,034	4,502	1,080	6,862	2,970	40,620
Camden	5.8%	5.9%	-0.1%	63,752	4,500	1,080	8,640	4,392	45,140
Cape May	1.1%	1.8%	-0.7%	20,085	4,500	1,080	4,500	1,080	8,925
Cumberland	1.8%	2.4%	-0.6%	25,848	4,500	1,080	4,500	1,080	14,688
Essex	8.9%	7.9%	1.0%	86,335	4,500	1,080	4,500	1,080	75,175
Gloucester	3.3%	3.6%	-0.3%	38,654	4,500	1,080	4,500	1,080	27,494
Hudson	7.2%	6.6%	0.6%	71,729	4,500	1,080	4,500	1,080	60,569
Hunterdon	1.4%	2.1%	-0.7%	23,024	4,500	1,080	4,515	1,093	11,836
Mercer	4.2%	4.3%	-0.1%	46,304	4,500	1,080	4,500	1,080	35,144
Middlesex	9.2%	8.2%	1.0%	88,937	4,500	1,080	4,500	1,080	77,777
Monmouth	7.2%	6.6%	0.6%	71,448	4,500	1,080	4,500	1,080	60,288
Morris	5.6%	5.3%	0.3%	58,236	4,500	1,080	4,500	1,080	47,076
Ocean	6.6%	6.1%	0.5%	66,165	4,500	1,080	4,500	1,080	55,005
Passaic	5.7%	5.4%	0.3%	59,113	4,500	1,080	4,500	1,080	47,953
Salem	0.8%	1.6%	-0.8%	17,099	4,500	1,080	4,500	1,080	5,939
Somerset	3.7%	4.0%	-0.3%	43,294	4,500	1,080	6,118	2,378	29,218
Sussex	1.7%	2.3%	-0.6%	25,086	4,500	1,080	4,500	1,080	13,926
Union	6.1%	5.8%	0.3%	63,450	4,500	1,080	5,782	2,106	49,982
Warren	1.2%	2.0%	-0.8%	21,463	4,500	1,080	4,842	1,354	9,687
Total	**100.0%**	**100.0%**	**10.9%***	**1,088,816**	**94,502**	**22,685**	**113,824**	**38,147**	**819,658**

*The sum of the absolute value of the difference between the population and vaccination proportions.

Under a limited budget level, the majority of the vaccines are allocated in Janssen, followed by Moderna, while Pfizer has the least number of vaccines allocated (Figure 6). This is because the insufficient budget limits the total number of vaccines purchased. The Janssen vaccine has the lowest price, followed by Moderna. Although Pfizer has the highest efficacy, the cost of each dose of the Pfizer vaccine is much higher than the others. Under the limited budget level (Table 2), the model chooses to vaccinate more people with mainly cheaper vaccines and vaccines with a single dose. The counties with a bigger population are more likely to receive more vaccines. However, all counties with a population proportion of more than 6% receive a lower proportion of vaccines than their population proportion, while all counties with a population proportion of less than 5% receive a proportion of vaccines that is higher than their population proportion. For example, Bergen County, with a population proportion of 10.3%, receives 9.5% of the total vaccines allocated. Other counties with a population proportion between 5% and 6% may receive more or less proportion of vaccines than their population due to their higher or fewer initial infections. Appendix Section A10 presents results for medium and ample budget levels.

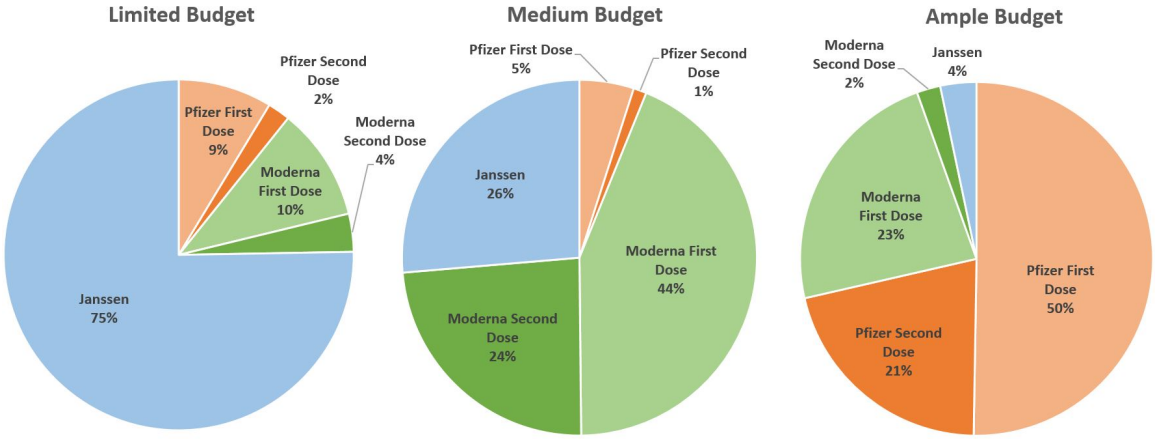

Figure 6: Proportion of each type of vaccine allocated under different budget levels.

When there is no budget limitation on vaccine allocation, vaccine efficacy is the only consideration for the vaccine administration. Thus, Pfizer vaccines have the priority to be allocated compared with Moderna and Janssen, as shown in Table A10 and Figure 6. Under the ample budget level, the vaccine allocation proportion is almost the same as the population proportion. For example, Bergen County receives 10.3% of the total vaccines, which is equivalent to its population proportion. This is because all people who are willing to be vaccinated receive the vaccine shots when the budget is

ample and as long as there is a sufficient vaccine supply. Furthermore, we assume the same vaccine acceptance rate in each county of New Jersey. As shown in Figure 6, for all the budget levels, the number of the second dose of Pfizer and Moderna vaccines is much smaller than that of the first dose. This is because when the total vaccine supply or vaccination capacity is bounded, even if the purchasing budget is ample, the model gives priority to administering as many as the first shots of those vaccines since the effectiveness of the first shot is high and more people can benefit from the vaccination.

3.2 Vaccination Center Location Decisions

In this subsection, we present the vaccination center location decisions generated by the model under the medium budget level. We also present results on the vaccination center locations for multiple types of vaccines in Appendix Section A11. We fixed the Pfizer vaccination center to one and Moderna and Janssen centers at zero, as shown on the left side of Figure 7.

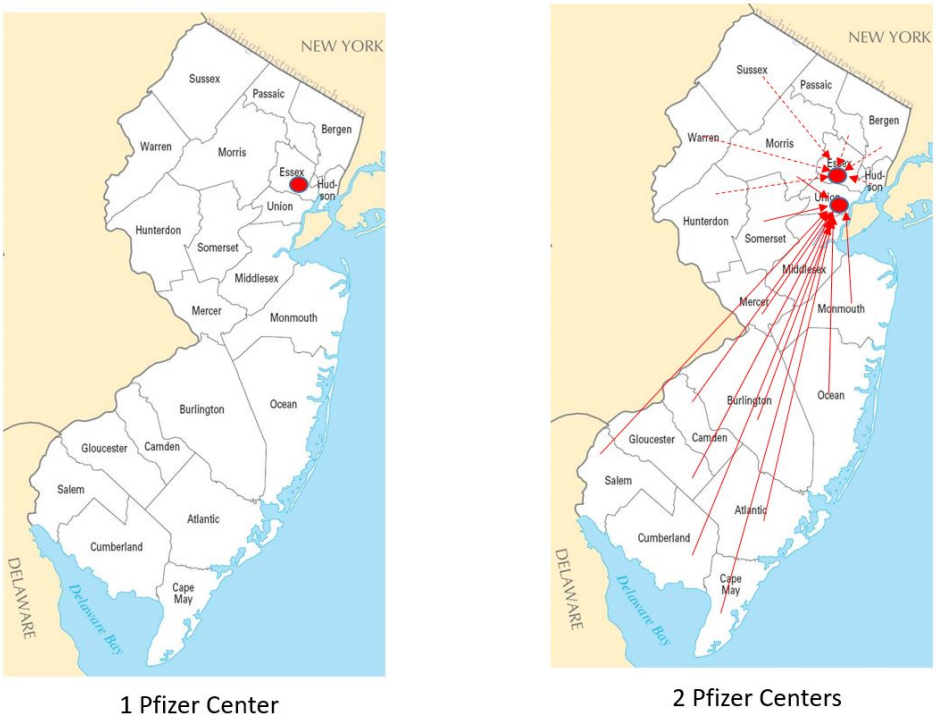

Figure 7: Vaccination center locations for Pfizer.

The model allocates the Pfizer center to Essex County, which is the same decision the government has taken in the real situation. We then increase the number of Pfizer vaccine centers to two, and the

vaccination center decision is changed. The right side of Figure 7 shows that one of the vaccination centers is allocated in Essex County, and the other is allocated in Union County. The vaccination center in Essex County serves Bergen County, Hudson County, Passaic County, Sussex County, Warren County, and Hunterdon County. The Union County vaccination center serves the rest of the counties in New Jersey. In Appendix Section A12, we present the results of vaccine allocation between the vaccination centers and local pharmacies (and small vaccination sites) when only one Pfizer center and different types of vaccination centers are located.

3.3 Sensitivity Analysis

We perform a sensitivity analysis to study the effect of the uncertainty in the underlying input parameters. The sensitivity analysis is done from the perspective of vaccine price, vaccine efficiency, and infection probability or transmission rate. We significantly change the base values of the parameters to observe considerable changes in results. Five scenarios are presented in the sensitivity analysis. Scenario "S1" represents a case in which the cost of Pfizer is between the cost of Moderna and Janssen. Specifically, we change the price of Pfizer to \$6.5 and the price of Moderna to \$1. Scenario "S2" represents a case where Pfizer has a lower cost than Moderna and Janssen. We achieve this scenario by changing the price of Pfizer to \$7.91, while keeping all other vaccines' costs at their original price. Scenario "S3" represents that Janssen has the highest efficiency, where we increase the efficiency of Janssen to 0.98 while reducing the efficiency of Pfizer and Moderna. Scenario "S4" represents that some regions have a higher transmission rate than others. We double the transmission rate for Atlantic County, Essex County, Hudson County, Middlesex County, Monmouth County, and Ocean County while keeping the transmission rates of others the same. Scenario "S5" represents the simulation-optimization results under all parameters' original values.

Figure 8 shows the cumulative infections, the total number of vaccines allocated, the number of vaccines allocated for each type (Pfizer, Moderna, and J&J, respectively), and the number of vaccines allocated to the vaccination centers under different scenarios. According to the results, total cumulative infections do not change much if we change the price or efficiency of the vaccines (see scenarios "S1," "S2," and "S3" versus "S5"). This result implies that the infection probability plays a more significant role than the vaccine cost and efficiency in the number of infections.

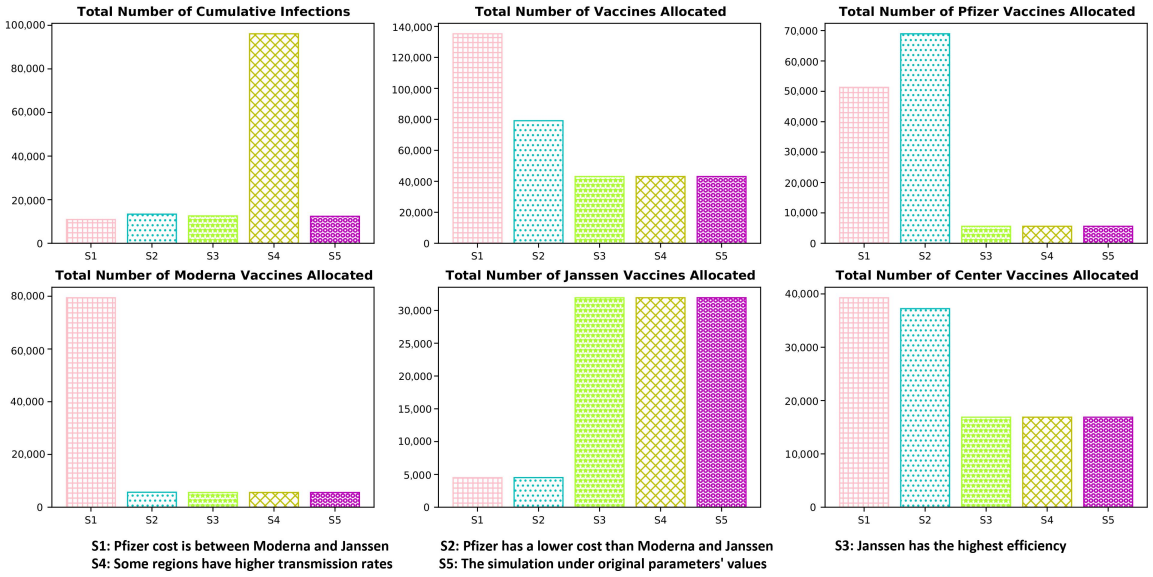

Figure 8: Sensitivity analysis under different scenarios.

The subfigures for the cumulative number of vaccines allocated and vaccines allocated for each type illustrate that more Pfizer vaccines are allocated under scenarios "S1" and "S2", and more Moderna vaccines are allocated under scenario "S1". Overall, the total number of vaccines allocated is more when the cost of vaccines is reduced, as expected. More vaccines are allocated to the vaccination centers when the cost of vaccines is reduced, compared to other scenarios that change the vaccine efficiency or infection probability, e.g., "S3" and "S4." These results reflect that the cost of vaccines plays a more critical role in vaccine allocations than vaccine efficiency. We also present results on giving vaccination priority to different age groups and incorporating vaccine storage costs in Appendix Section A13.

4 Discussion and Future Directions

In this study, we formulate a simulation-optimization model to generate the vaccination center locations for different types of vaccines and the optimal vaccine allocation strategies among different regions. We extend the agent-based simulation model presented by Kerr et al. (2021) by adding two vaccination compartments. The simulation model is able to incorporate the vaccination for the three types of vaccines, which are the first and second shots for Pfizer and Moderna, and the single dose for Janssen. The simulation model simulates the number of susceptible individuals and infections

for a certain time period and imports the results into the optimization model. The optimization model incorporates an SVIR simulation model, the available budgets, and potential vaccination center locations, as well as the total number of vaccines available and the willingness of people to get vaccinated to generate the optimal vaccination center location and vaccine allocation strategies for each county in the future planning horizon. Then the generated results are used as the inputs of the simulation model to estimate the number of infections and various disease compartmental values with the vaccination strategies for the same period. We apply our model to the case of vaccine allocation among all the counties in New Jersey State.

First, we validate our model with the real outbreak data. The predicted results fit the real outbreak data well, and the paired t-test shows that our predicted results have no statistically significant difference from the real outbreak data. We also note that the unbiased number of infections might be higher than the reported cases (Omori et al., 2020). Since the majority of unnoticed cases are non-severe or asymptomatic, we assume that those would not cause a heavy burden on the healthcare systems. Therefore, we did not adjust the estimation of infections in regard to unbiased estimations. However, this could be a meaningful future direction for this work. We test our model on the cumulative number of infections under different budget levels. The results indicate that there is at least a month to see the difference in the number of infections under different budget levels since it takes time for vaccination impacts to take effect in reducing infections. In addition, the county with a high population and initial infections usually receives more vaccines allocated. For all the budget levels, the model allocates more first doses than second doses for Pfizer and Moderna vaccines. This is because more people benefit from taking the first shot of the vaccines when the vaccine supply or vaccination capacity is limited.

The number of vaccines allocated increases with the increase in the available budget. Under limited budgets, more vaccines with a lower unit cost should be allocated because the limited budget reduces the number of vaccinated people compared with other budget levels. Using a low-cost vaccine, more people are vaccinated, and the number of infections is minimized. The counties with higher population proportions are more likely to have higher vaccine allocation proportions since the model gives priority to vaccinating people in these regions. Under the medium budget level, more vaccines with higher costs and higher efficacy are allocated. The model has the flexibility to allocate those highly efficient vaccines due to the increased budget, but there is still a limitation

on the number of vaccines distributed since the budget is still not ample enough. The counties with a higher population will receive even more vaccines due to the high number of infections. Under the ample budget level, there is no limitation on the vaccine cost. Two main factors that influence vaccine allocation are the vaccine acceptance rate by people and the available vaccine supply. In this case, the model allocates as many high-efficacy vaccines as possible to minimize the total number of infections. The total number of people being vaccinated under an ample budget level is bounded by the people who are willing to be vaccinated since the vaccine supply is also relatively abundant. We have also statistically shown that the number of cumulative infections would be lower in each region as more vaccines are available. Another interesting result is that the gap between the population and vaccination proportions gets smaller as we increase the budget. Under the ample budget level, the vaccine allocation proportion is almost the same as the population proportion, while the absolute value of the differences between those proportions can sum up to 10.9% under a limited budget. Thus, it is more critical to use our simulation-optimization approach to fine-tune the vaccine allocation decisions under a limited budget or a limited vaccine supply.

The results of vaccination center locations show that the model gives priority to allocating vaccine centers to the region that has the closest distance to the vaccine supply warehouse. When more vaccine centers are included, the centers are located by order of distance to the vaccine warehouse from the shortest to the longest. When only allowing one type of vaccination center allocated in each county, the model prioritizes the type of center with a higher vaccine efficacy and then the centers with a lower efficacy. We also find that the allocation of vaccines moves from the vaccination centers to pharmacies and small vaccine sites when the budget is increased from limited to ample, consistent with what happened in the real case. When vaccines were newly available and limited, most people had to travel to vaccine centers for mass vaccination. As vaccines become more available, most vaccines are distributed to local pharmacies so that people can get immunization in their own counties (Gharpure et al., 2021). The sensitivity analysis indicates that the infection probability influences the number of infections more than vaccine cost and efficiency. Thus, non-pharmaceutical interventions, e.g., masks, social distancing, and closures, are still needed in addition to vaccines when the transmission situation of the disease becomes worse, consistent with the results of former research (see e.g., Shen et al. (2021)). The vaccine cost is more important than the vaccine efficiency when deciding the number of vaccines allocated because most developed

vaccines for COVID-19 have a relatively high-efficiency level. A reduction in vaccine costs is needed for higher vaccine coverage, which may then reduce the disease's death rate.

The optimization model could be extended by incorporating equitable vaccine allocation over multiple regions. There is no universal consensus on the definition and measurement of equity in public healthcare decision-making (Lane et al., 2017). One can define equity in the context of the vaccine location-allocation problem as the case where each region receives its fair share of vaccines with respect to its population, similar to the capacity equity metric defined in Yin and Büyüktahtakın (2021). Without equity constraints, the positive and negative deviations between the population and vaccination proportions are shown in Tables 2, A9, and A10 under limited, medium, and high budgets, respectively. As shown in Table A9, the sum of the absolute value of the difference between the population and vaccination proportions for each county under the medium budget is only 3.4%, and it is only 0.4% in Table A10 under the ample budget. This result implies that our model balances the proportional vaccine distribution with a county's population in proportion to all counties considered. This is because our spatio-temporal optimization formulation, incorporating simple SVIR and very detailed agent-based models, oversees the spread among multiple regions and optimizes vaccine allocation not only for a specific county but over all counties and throughout the planning horizon. The deviations are the highest when the budget is limited. Imposing equity constraints would reduce the deviations with a potential cost of increased total infections over all counties under very tight budgets. Future work can define different equity measures, either based on specific groups, e.g., Black and Hispanic populations most impacted by COVID-19 (Burks et al., 2020), or geographical areas that do not receive a fair share of vaccine or treatment resources.

The limitations of the optimization and simulation models and potential future extensions of this work can be described in the following ways. First, our optimization model considers the potential vaccination center locations and each region's overall capacity of local pharmacies. The specific distribution from the warehouse to each of the local pharmacies in each county is not included to not further complicate the model. In a future study, the local pharmacy supply chain and vaccine distribution over all pharmacies in a region can be incorporated. In such a detailed vaccine distribution problem, various vaccine transportation, storage modes, temperatures, and associated costs could be integrated into the model. Furthermore, in our case study, we use the real locations of the vaccine warehouse. Since the distance from the warehouse to the vaccination centers is the

main factor that influences the vaccination center locations, the model chooses the closest county to the supply warehouse for each vaccine type as the corresponding vaccination center, despite the impact of the infection rate in each region. However, a future extension of this study could make the vaccine center locations more sensitive by incorporating a local supply chain and variable locations and numbers of vaccine warehouses (e.g., the vaccine warehouse location can be decided by the population or number of infections, and it can be changed for different time periods). In addition, our model assumes that the people in each county can only be served by the vaccine centers located in the closest county. In a real situation, human behavior is hard to capture, and some people may go to other places to receive vaccines due to the complex environment. Thus, various human behaviors that could impact vaccination policies could be incorporated into the model.

While the agent-based simulation considers demographic differences, such as age, and the impact of different contact networks on disease transmission, the educational, social, and economic disparities among human populations could be explicitly incorporated into the model. Given the availability of the data, regions could be made more heterogeneous by including different socio-economic levels and varying vaccination and vaccine acceptance rates. Furthermore, specific variants and waning immunity of the infected or vaccinated population could be integrated into the models to capture further biological complexities of the disease. Our model only considers the overall vaccination strategies for the people against the spread of the disease. It would be interesting to study the specific vaccination strategies based on different risk groups and super spreaders. For instance, one may fix the number of vaccines but compare vaccination strategies targeting random people or age-based groups or groups with specific medical conditions.

Data and Code Availability Statement

All input data used is presented either within the manuscript or its appendix. The codes generated and data used are available at Yin et al. (2023a).

Acknowledgements

The authors acknowledge the generous support from the National Science Foundation CAREER Award co-funded by the CBET/ENG Environmental Sustainability program and the Division of Mathematical Sciences in MPS/NSF under Grant No. CBET-1554018.

References

Ambikapathy, B. and Krishnamurthy, K. (2020). Mathematical modelling to assess the impact of lockdown on COVID-19 transmission in India: Model development and validation. *Journal of Medical Internet Research (JMIR) Public Health and Surveillance*, 6(2):e19368.

Bertsimas, D., Digalakis Jr, V., Jacquillat, A., Li, M. L., and Previero, A. (2021). Where to locate COVID-19 mass vaccination facilities? *Naval Research Logistics (NRL)*.

Burks, C. A., Ortega, G., and Bergmark, R. W. (2020). COVID-19 , disparities, and opportunities for equity in otolaryngology—unequal america. *JAMA Otolaryngology–Head & Neck Surgery*, 146(11):995–996.

Bushaj, S., Yin, X., Beqiri, A., Andrews, D., and Büyüktahtakın, İ. E. (2022). A simulation-deep reinforcement learning (SiRL) approach for epidemic control optimization. *Annals of Operations Research*, pages 1–33.

Büyüktahtakın, İ. E. (2022). Stage-t scenario dominance for risk-averse multi-stage stochastic mixed-integer programs. *Annals of Operations Research*, 309(1):1–35.

Büyüktahtakın, İ. E. (2023). Scenario-dominance to multi-stage stochastic lot-sizing and knapsack problems. *Computers & Operations Research*, page 106149.

Büyüktahtakın, İ. E., des Bordes, E., and Kıbış, E. Y. (2018). A new epidemics–logistics model: Insights into controlling the Ebola Virus Disease in West Africa. *European Journal of Operational Research*, 265(3):1046–1063.

Carr, S. and Roberts, S. (2010). Planning for infectious disease outbreaks: A geographic disease spread, clinic location, and resource allocation simulation. In *Proceedings of the 2010 Winter Simulation Conference*, pages 2171–2184. IEEE.

CDC (2022). Vaccines.gov. https://www.vaccines.gov/. Accessed July 4, 2022.

Coşgun, Ö. and Büyüktahtakın, İ. E. (2018). Stochastic dynamic resource allocation for HIV prevention and treatment: An approximate dynamic programming approach. *Computers & Industrial Engineering*, 118:423–439.

Dasaklis, T. K., Pappis, C. P., and Rachaniotis, N. P. (2012). Epidemics control and logistics operations: A review. *International Journal of Production Economics*, 139(2):393–410.

Ekici, A., Keskinocak, P., and Swann, J. L. (2014). Modeling influenza pandemic and planning food distribution. *Manufacturing & Service Operations Management*, 16(1):11–27.

FEMA (2022). Federally supported community vaccination centers. https://www.fema.gov/disaster/coronavirus/vaccine-support/vaccine-center. Accessed July 4, 2022.

Gharpure, R., Guo, A., Bishnoi, C. K., Patel, U., Gifford, D., Tippins, A., Jaffe, A., Shulman, E., Stone, N., Mungai, E., et al. (2021). Early COVID-19 first-dose vaccination coverage among residents and staff members of skilled nursing facilities participating in the pharmacy partnership for long-term care program—United States, December 2020–January 2021. *Morbidity and Mortality Weekly Report*, 70(5):178.

Heffernan, E. (2021). COVID-19 vaccine distribution allocations by jurisdiction - Pfizer. https://data.cdc.gov/Vaccinations/COVID-19-Vaccine-Distribution-Allocations-by-Juris/saz5-9hgg. Accessed June 10, 2021.

JHU (2020). COVID-19 United States Cases by County. https://coronavirus.jhu.edu/us-map. Accessed November 30, 2020.

JHU (2021). COVID-19 dashboard. https://coronavirus.jhu.edu/map.html. Accessed July 10, 2021.

Kaplan, E. H., Craft, D. L., and Wein, L. M. (2003). Analyzing bioterror response logistics: the case of Smallpox. *Mathematical Biosciences*, 185(1):33–72.

Kerr, C. C., Stuart, R. M., Mistry, D., Abeysuriya, R. G., Rosenfeld, K., Hart, G. R., Núñez, R. C., Cohen, J. A., Selvaraj, P., Hagedorn, B., et al. (2021). Covasim: an agent-based model of COVID-19 dynamics and interventions. *PLOS Computational Biology*, 17(7):e1009149.

Kibis, E., Büyüktahtakın, İ. E., Haight, R. G., Akhundov, N., Knight, K., and Flower, C. (2020). A new multi-stage stochastic programming model and cutting planes for the optimal surveillance and control of emerald ash borer in cities. *INFORMS Journal on Computing*, 33(2):808–834.

Lane, H., Sarkies, M., Martin, J., and Haines, T. (2017). Equity in healthcare resource allocation decision making: a systematic review. *Social Science & Medicine*, 175:11–27.

Lee, B. Y., Brown, S. T., Korch, G. W., Cooley, P. C., Zimmerman, R. K., Wheaton, W. D., Zimmer, S. M., Grefenstette, J. J., Bailey, R. R., Assi, T.-M., et al. (2010). A computer simulation of vaccine prioritization, allocation, and rationing during the 2009 H1N1 influenza pandemic. *Vaccine*, 28(31):4875–4879.

Liu, X., Takeuchi, Y., and Iwami, S. (2008). SVIR epidemic models with vaccination strategies. *Journal of Theoretical Biology*, 253(1):1–11.

NJ.GOV (2021). COVID-19 vaccine. https://covid19.nj.gov/pages/vaccine. Accessed July 10, 2021.

NJIT (2021). NJIT to host community COVID-19 vaccination center. https://news.njit.edu/njit-host-community-covid-19-vaccination-center. Accessed June 10, 2021.

Nsoesie, E. O., Beckman, R. J., Shashaani, S., Nagaraj, K. S., and Marathe, M. V. (2013). A simulation optimization approach to epidemic forecasting. *PloS One*, 8(6):e67164.

Omori, R., Mizumoto, K., and Nishiura, H. (2020). Ascertainment rate of novel Coronavirus disease (COVID-19) in Japan. *International Journal of Infectious Diseases*, 96:673–675.

Onal, S., Akhundov, N., Büyüktahtakın, İ. E., Smith, J., and Houseman, G. R. (2020). An integrated simulation-optimization framework to optimize search and treatment path for controlling a biological invader. *International Journal of Production Economics*, 222:107507.

Peter Loftus, P. V. (2021). Vaccine manufacturing issues force Moderna to cut supplies to Canada, U.K. https://www.wsj.com/articles/vaccine-manufacturing-issues-force-moderna-to-cut-supplies-to-canada-u-k-11618600046. Accessed July 10, 2021.

Pfizer (2021). Manufacturing and distributing the COVID-19 vaccine. https://www.pfizer.com/science/coronavirus/vaccine/manufacturing-and-distribution. Accessed July 10, 2021.

Queiroz, M. M., Ivanov, D., Dolgui, A., and Fosso Wamba, S. (2022). Impacts of epidemic outbreaks on supply chains: mapping a research agenda amid the covid-19 pandemic through a structured literature review. *Annals of operations research*, 319(1):1159–1196.

Saldaña, F., Flores-Arguedas, H., Camacho-Gutiérrez, J. A., and Barradas, I. (2020). Modeling the transmission dynamics and the impact of the control interventions for the COVID-19 epidemic outbreak. *Mathematical Biosciences and Engineering*, 17(4):4165–4183.

Shamil, M. S., Farheen, F., Ibtehaz, N., Khan, I. M., and Rahman, M. S. (2021). An agent-based modeling of COVID-19: validation, analysis, and recommendations. *Cognitive Computation*, pages 1–12.

Shen, M., Zu, J., Fairley, C. K., Pagán, J. A., An, L., Du, Z., Guo, Y., Rong, L., Xiao, Y., Zhuang, G., et al. (2021). Projected COVID-19 epidemic in the united states in the context of the effectiveness of a potential vaccine and implications for social distancing and face mask use. *Vaccine*, 39(16):2295–2302.

Tanner, M. W., Sattenspiel, L., and Ntaimo, L. (2008). Finding optimal vaccination strategies under parameter uncertainty using stochastic programming. *Mathematical Biosciences*, 215(2):144–151.

WHO (2021). Costs of delivering COVID-19 vaccine in 92 AMC countries. https://www.who.int/publications/m/item/costs-of-delivering-covid-19-vaccine-in-92-amc-countries. Accessed June 10, 2021.

Yin, X., Bushaj, S., Yue, Y., and Büyüktahtakın, İ. E. (2023a). COVID-19: Simulation-optimization model codes and data for vaccine center location and vaccine allocation. https://doi.org/10.5281/zenodo.8002371.

Yin, X. and Büyüktahtakın, İ. E. (2021). A multi-stage stochastic programming approach to epidemic resource allocation with equity considerations. *Health Care Management Science*, 24(3):597–622.

Yin, X. and Büyüktahtakın, İ. E. (2022). Risk-averse multi-stage stochastic programming to optimizing vaccine allocation and treatment logistics for effective epidemic response. *IISE Transactions on Healthcare Systems Engineering*, 12(1):52–74.

Yin, X., Büyüktahtakın, İ. E., and Patel, B. P. (2023b). COVID-19: Data-driven optimal allocation of ventilator supply under uncertainty and risk. *European Journal of Operational Research*, 304(1):255–275.

Zaric, G. S. and Brandeau, M. L. (2001). Resource allocation for epidemic control over short time horizons. *Mathematical Biosciences*, 171(1):33–58.